

C-MAC: Model-driven Concurrent Medium Access Control for Wireless Sensor Networks

Mo Sha¹; Guoliang Xing²; Gang Zhou³; Shucheng Liu¹; Xiaorui Wang⁴

¹City University of Hong Kong, ²Michigan State University, USA

³College of William and Mary, USA, ⁴University of Tennessee, Knoxville, USA

Abstract—This paper presents C-MAC, a new MAC protocol designed to achieve high-throughput bulk communication for data-intensive sensing applications. C-MAC exploits concurrent wireless channel access based on empirical power control and physical interference models. Nodes running C-MAC estimate the level of interference based on the physical Signal-to-Interference-plus-Noise-Ratio (SINR) model and adjust the transmission power accordingly for concurrent channel access. C-MAC employs a block-based communication mode that not only amortizes the overhead of channel assessment, but also improves the probability that multiple nodes within the interference range of each other can transmit concurrently. C-MAC has been implemented in TinyOS-1.x and extensively evaluated on Tmote nodes. Our experiments show that C-MAC significantly outperforms the state-of-art CSMA protocol in TinyOS with respect to system throughput, delay and energy consumption.

I. INTRODUCTION

Recently Wireless Sensor Networks (WSNs) have been deployed for several *data-intensive* sensing applications such as structural monitoring [23] and habitat monitoring [20]. Nodes in these applications must sample the physical environments at high rates. For instance, accelerometers must sample the vibration of a structure at more than 100 Hz in order to detect potential defects [23]. Due to the limited storage capacity of sensor nodes, the accumulated data should be periodically delivered to the base station for offline analysis [23].

Data-intensive applications pose several major challenges to the design of WSNs. Sensor nodes have very limited bandwidth due to tight power budget. In many scenarios, sensor data must be delivered to the sink through multiple hops. The achievable delivery rate is thus limited by the interference among transmitting nodes. As a result, a fundamental tension exists between the sheer amount of data generated by nodes and the low communication capacity of WSNs. Moreover, the low network throughput also leads to poor energy efficiency as nodes must remain active for a long period of time.

The efficiency of Media Access Control (MAC) plays a key role in the achievable throughput of a wireless network. The primary design goal of existing WSN MAC protocols is energy efficiency. CSMA-based MACs (e.g., S-MAC [24], T-MAC [21], B-MAC [12] and WiseMac [5]) reduce collisions by carrier sensing and distributed channel reservation. To reduce idle listening time of radios, nodes may be put into sleep synchronously [21] [24] or in an on-demand fashion [5] [12]. TDMA-based MACs (e.g., TRAMA [13], DCQS [4] and

DRAND [16]) divide time into slots and allocate them to all nodes within the interference range. There also exist hybrid protocols (e.g., SCP [25] and Funneling-MAC [1]) that combine the advantages of TDMA and CSMA protocols.

Although a number of MAC protocols exist for WSNs, they are not designed to achieve high throughput for data-intensive sensing applications. CSMA-based MACs prevent multiple nodes within the interference range from concurrently accessing the channel, which severely limits the achievable throughput of multi-hop WSNs. TDMA-based MACs, on the other hand, incur high maintenance overhead as the schedules of nodes are sensitive to changes in network traffic or network topology. This paper presents a new MAC protocol called C-MAC that is designed to achieve high-throughput bulk communication for data-intensive sensing applications. The key novelty of C-MAC is the exploitation of concurrent channel access based on *empirical* power control and interference models. By boosting the system throughput, C-MAC also improves the energy efficiency of a network as nodes can be turned off for a longer period.

Our experiments on Tmote nodes reveal that a wide transitional region exists in the correlation between Packet Reception Ratio (PRR) and Signal-to-Interference-plus-Noise-Ratio (SINR). By taking advantage of this transitional relationship between PRR and SINR, C-MAC enables multiple nodes to transmit concurrently although they are within the interference range of each other. Specifically, each node running C-MAC maintains a power control model and a physical SINR model that are used for predicting the opportunity of accessing the channel together with other transmitting nodes. To mitigate the negative impact of increased interference due to concurrent transmissions, C-MAC carefully chooses the transmit power of senders such that the local throughput of active links within the interference range is maximized. C-MAC has been implemented in TinyOS-1.x and extensively evaluated on Tmote nodes. Our experiments based on a 16-node test-bed show that C-MAC improves the system throughput under the CSMA-based B-MAC [12] by more than twice.

The rest of the paper is organized as follows. Section II reviews related work. Section III motivates the approach of concurrent transmissions through experiments. We discuss empirical power control and interference models in Section IV. The design and implementation of C-MAC are presented in Section V. Experimental results are offered in Section VI. We conclude the paper in Section VII.

II. RELATED WORK

Existing WSN MAC protocols fall into two basic categories: Carrier Sense Multiple Access (CSMA) based and Time Division Multiple Access (TDMA) based protocols. The primary design goal of the existing WSN MAC protocols is to achieve network energy efficiency through radio sleep scheduling.

S-MAC [24] is a typical CSMA protocol that avoids collisions through distributed channel arbitration. Nodes within transmission range of one another synchronize their schedules to ensure that they are all awake at the same time. T-MAC [21] extends S-MAC by allowing nodes to adaptively turn off their radios if no traffic is detected. Different from S-MAC and T-MAC, another type of CSMA-based MAC protocols (such as B-MAC [12], X-MAC [3], and WiseMac [5]) does not require synchronous contention periods. Transmitting nodes send a stream of preamble bytes equal to the polling period of their receivers in order to ensure that they wake up in time.

TDMA-based protocols divide time into time slots and allocate to all nodes within transmission range of one another. Nodes transmit during their own time slots and listen during the time slots when they wish to receive. Several different TDMA-based protocols have been proposed for WSNs, including TRAMA [13], DCQS [4], and DRAND [16].

Hybrid protocols (such as SCP [25], Funneling-MAC [1] and Z-MAC [15]) attempt to combine some of the advantages of TDMA and CSMA protocols. For example, Funneling-MAC allows the nodes close to the sink to run TDMA schedules while all others follow either a scheduled contention or polling based duty cycle. We note that the hybrid approach is complementary to the design of C-MAC. In particular, the channel concurrency mechanism employed by C-MAC not only enables interfering nodes to transmit at the same time in a CSMA protocol, but also allows them to share the same time slot in TDMA protocols, which leads to a higher system throughput.

Several power control MACs [7] [11] have been designed to achieve better spatial reuse in wireless ad hoc networks. However, the design principles of these traditional power control MACs are fundamentally different from that of C-MAC. First, the threshold-based carrier sensing mechanisms are usually used to adjust the transmission power for better spatial reuse. In contrast, C-MAC completely disables carrier sensing and predicts the throughput of on-going transmissions based on empirical PRR-SINR model. Second, traditional MACs employ per-packet handshakes for collision avoidance. Although such a strategy is effective for high-rate radios (like 802.11 radios), it will incur significant overhead for low-rate radios in WSNs. Moreover, these MACs rely on several idealistic assumptions such as symmetric power attenuation and binary relationship between SINR and packet reception. However, the experimental results from our work and recent empirical studies [10] largely invalidate these assumptions. Different from these simulation-based MACs, C-MAC is designed based on empirical models and evaluated on real-world sensor network platforms.

Son et al. [18] [19] modeled the transitional region in the relationship between PRR and SINR based on the CC1000

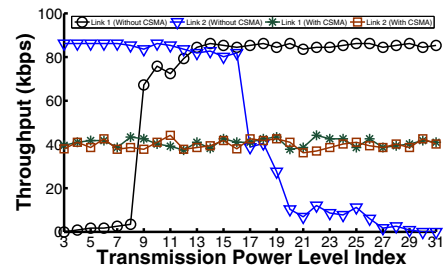


Fig. 1. The throughput of two interfering links.

radio. They concluded that the SINR threshold for successful packet reception is dependent on both received signal strength (RSS) and number of interferers. However, the findings of this work based on the newer CC2420 radio platform show that the transitional region does not have a strong correlation with either RSS or the number of interferers after accounting for measurement errors. In particular, the correlation between PRR and Signal-to-Noise-Ratio (SNR) is shown to well approximate that between PRR and SINR while the former can be measured with significantly lower overhead.

Several practical models [8] [14] have been proposed to predict the throughput of multiple nodes under the physical interference models in 802.11 networks. However, little work has been done to apply these models in protocol design. Several studies [2] [6] [9] investigate efficient algorithms of link scheduling and routing based on the physical interference model. However, these algorithms are not implemented or evaluated on real wireless platforms.

A recent study [22] proposed to increase concurrent transmissions in 802.11 networks by utilizing the transmission conflict maps learned by nodes. However, as nodes use fixed transmission power, the opportunity of concurrent transmissions cannot be fully explored for a given network topology. Moreover, such an approach is opportunistic in nature as it does not control the success rate of concurrent transmissions. In contrast, C-MAC can accurately predict such success rate based on empirical power control and interference models and adapt the transmission power of nodes to maximize it.

III. A CASE OF CONCURRENT TRANSMISSIONS

In this section, we demonstrate the advantage of concurrent transmission through an experiment using four Tmote nodes. Nodes s_1 and s_2 transmit to r_1 and r_2 at the highest speed, respectively. s_2 's transmit power is set to be 15 (-7 dBm) while s_1 increases its power level from 3 (-25dBm) to 31 (0dBm). To study the performance of concurrent transmissions under interference, r_2 and r_1 are intentionally placed within the interference range of s_1 and s_2 , respectively. In the first run of experiments, senders run the default CSMA protocol in TinyOS-1.x. In the second run of experiments, the clear channel assessment (CCA) is disabled to allow two senders to transmit concurrently under interference.

Figure 1 shows the throughput of Link 1 (from s_1 to r_1) and Link 2 (from s_2 to r_2). When CSMA is employed, both

links achieve a throughput about 40 kbps. As s_1 and s_2 can sense each other's transmission, they have roughly equal time of accessing the channel. With CSMA disabled, the two links yield significantly different throughputs when s_1 varies its transmission power. When the transmit power level of s_1 is smaller than 9, the throughput of link 1 is lower than 10 kbps due to the severe interference from s_2 . The throughput drastically increases to 68 kbps when the transmit power level reaches 9 as s_1 's packets have higher signal strength than the interfering packets from s_2 . The throughput of Link 1 continues to grow to 88 kbps because of the increasing SINR at r_1 . When the transmit power level of s_1 is greater than 16, the throughput of link 2 drops significantly due to the strong interference from s_1 . Overall, Figure 1 shows the existence of a wide region in which both links achieve significantly higher throughputs by disabling CSMA. This result clearly demonstrates the advantage of concurrent transmissions.

IV. EMPIRICAL POWER CONTROL AND INTERFERENCE MODELS

In this section, we discuss empirical power control and interference models. We first describe our experimental settings in Section IV-A. We then describe our RSS and SINR models in Section IV-B and IV-C, respectively.

A. Experimental Methodology

Our experiments are conducted on a test-bed composed of 16 Tmote Sky motes. Each mote is equipped with an IEEE 802.15.4 compliant Chipcon CC2420 radio. The maximum bit rate is 250 kbps. The CC2420 radio has 31 transmit power levels between -25 to 0 dBm. The Received Signal Strength Indicator (RSSI) of CC2420 contains the measurement of signal power (in the unit of dBm) averaged over a 32-bit period (128us) and is continuously updated. When there are no incoming packets, the RSSI value is the signal power of environmental noise. The Received Signal Strength (RSS) of an incoming packet can be either read directly from the RSSI register or from the metadata in the packet. The default CSMA-based MAC protocol in TinyOS-1.x, B-MAC [12] is used in our experiments. We intentionally disabled carrier sense, ACK and random backoff in the MAC implementation. To investigate the spatial impact, we carry out experiments in four different environments: an office, a corridor, a grass field and an open parking lot as shown in Figure 2.

B. Transmit Power vs. Received Signal Strength

We first study the correlation between transmit power of senders and the RSS measured by receivers. The empirical study in [10] showed that such correlation is nearly linear. Denote $RSS(v, u, P_u)$ as the RSS measured by node v when node u transmits at power P_u . Then we have [10]:

$$RSS(v, u, P_u) = A_{u,v} \times P_u + B_{u,v} \quad (1)$$

where $A_{u,v}$ and $B_{u,v}$ are two time-varying constants dependent on environment.



Fig. 2. Four environments used for measurements.

To evaluate the accuracy of the linear model in (1), we conduct the following experiments. A mote is placed at a fixed position and serves as the sender. Another mote serves as the receiver and is placed at different distances from the sender. In each configuration, the sender transmits 100 packets at each transmit power level from 1 to 31. The receiver records the average RSSI values of received packets. Each experiment is repeated for 10 runs. The variance is in a very small range and the degree is related to the environment.

Figure 3 shows RSS versus transmit power in different environments. Several observations can be drawn from the results. First, RSS grows nearly linearly in all environments¹. Second, the correlation between transmit power and RSS varies significantly in different environments. In particular, the attenuation of transmit power in outdoor environments (grass field and parking lot) is much higher than that in indoor environments (office and corridor). Third, transmit power does not yield a linear correlation with distance in logarithmic scale.

We also studied the temporal impact by repeating the experiments at different times. We observed that the correlation between transmit power and RSS changes over time. However, a similar linear relationship between them always holds. This observation is consistent with the results in a previous study [10]. Due to the space limitations, the experimental results on temporal impact are not shown here and can be found in [17].

C. Packet Reception Ratio vs. SINR

1) *Measurement methodology*: In the second set of experiments, we measure the physical interference model, i.e., the correlation between PRR and SINR. The experiments were carefully designed under a range of conditions including different environments, signal strengths, and numbers of interferers. Two nodes in the experiments serve as the sender and receiver, respectively. A number of other nodes serve as jammers whose transmissions interfere with the packet reception of the receiver. The nodes are placed on the floor of an office. To create different interference conditions, we vary the positions of the jammers and the transmit power of the sender and jammers. Moreover, packet transmissions of sender and jammers must be precisely scheduled in order to obtain desired SINR levels.

¹There exists a non-linear region in the RSS measurements in the office and corridor. However, the transmit power levels in the region are small and can be safely ignored in practice.

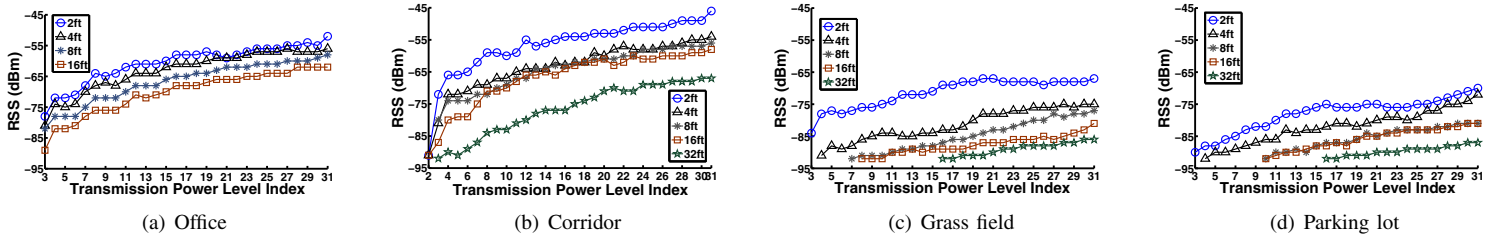


Fig. 3. RSS measurements in four environments.

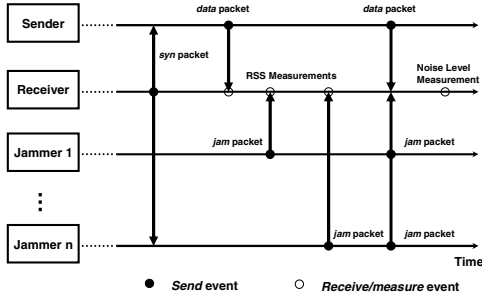


Fig. 4. Sequence of packet transmissions.

Figure 4 illustrates the sequence of packet transmissions in our measurements. The experiment starts with the receiver broadcasting a *syn* packet. After receiving the packet, the sender and jammers start two timers TimerA and TimerB. A node transmits a packet when either TimerA or TimerB fires. The timeouts of TimerAs are staged such that the packets transmitted by the sender and jammers do not collide. However, the timeout of TimerB is set to be the same for each node such that their packets collide at the receiver. The receiver measures the energy of environmental noise after all packet transmissions. This process is repeated for 1000 times and the packet reception ratio of the receiver is calculated based on the number of packets received. If a packet is successfully received, the receiver records its RSS value. Note that the measured RSS is the total energy of environmental noise and the signals from both the sender and jammers. Therefore, the strength of interfering signals cannot be obtained from the RSS of collided packets. In order to obtain the SINR at the receiver, the strength of interference is measured without collisions, i.e., the RSS of the packets transmitted by jammers when their TimerAs fire.

2) *Measurement results:* We measure PRR vs. SINR under a range of conditions including different environments, signal strengths, and numbers of jammers. Due to space limitations, we only report the results obtained from an office with different numbers of jammers; and other results can be found in [17].

Figure 5(a) shows PRR vs. SINR with different numbers of jammers. The transmit power of sender is -10 dBm. When there is no jammer, the result illustrates the relationship between PRR and SNR. As shown in Figure 5(a), the relationship between PRR and SINR (or SNR) yields a transitional region about 4 dB in all three settings, where the PRR quickly increases from 0 to 100%. Such a probabilistic packet reception performance has

also been observed in several previous empirical studies [26]. Moreover, it can be seen that the variation of the relationship between PRR and SINR increases with the number of jammers. This result is mainly caused by the system errors in the measurements explained as follows.

As discussed in Section IV-C.1, the strength of interfering signals cannot be directly measured as the RSSI reading of a received packet is the total energy of environmental noise and the signals from both the sender and jammers. In order to calculate the SINR at the receiver, the strength of interference is measured as the RSS of packets sent by jammers *before* the collision. We now analyze the possible system errors introduced by this method. The size of packets used in the measurements is 100 bytes². The time for receiving a packet is about 4 *ms*. However, as we observed from experiments, the delay between the timeout of a sending timer and the actual time instance that a packet is sent from the radio buffer could be as high as 2 *ms* due to timer and packet processing overhead. Consequently, jamming packets may not always collide with the sender's packet at the receiver. Therefore, the total energy of jamming packets (which is measured separately before the collision) could be different from the actual strength of interference. Moreover, the discrepancy increases with the number of jammers. As a result, the relationship between SINR and PRR yields a higher variation in presence of more jammers.

We also measured PRR versus SINR with different RSS values. The results are similar to Figure 5(a) except that the variation of the relationship between PRR and SINR decreases with the value of RSS. This is due to the smaller impact of environmental noise when signal strength becomes higher. Due to space limitations, the results are omitted here and can be found in [17]. In summary, our measurements show that the relationship between PRR and SINR (SNR) yields a transitional region about 4 dB. Moreover, considerable variations are observed under different transmit powers and numbers of jammers. However, the variations are mainly caused by the environmental noise and system errors in the measurements. We note that reducing the measurement errors on motes is challenging due to a number of factors such as the limited precision level of RSSI registers and unpredictable software overhead of packet processing.

To capture the transitional region of the relationship between PRR and SINR, we developed a clustered probabilistic model

²The CC2420 radio supports a maximum packet size of 128 bytes.

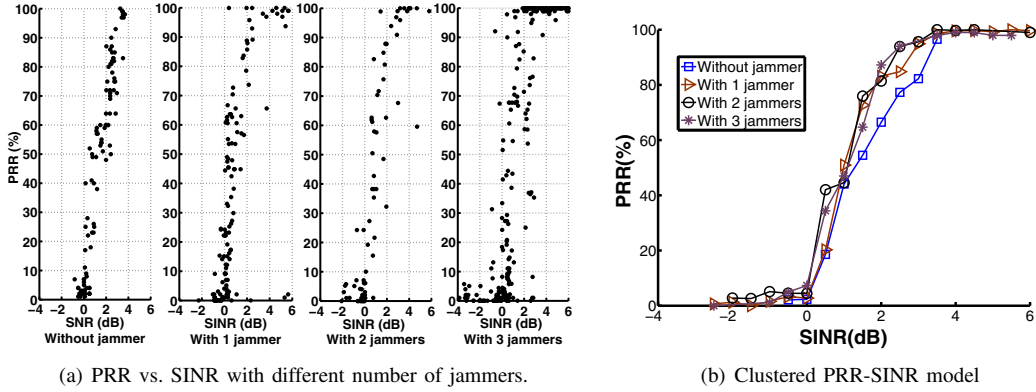


Fig. 5. PRR vs. SINR with different number of jammers and the clustered PRR-SINR model.

as follows. Suppose the transitional region of node u is $[0, D]$ dB and $T = \{(SINR_u(i), PRR_u(i)) \mid SINR_u(i) \in [0, D]\}$ denotes the set of SINR-PRR measurements of receiver u . We evenly divide $[0, D]$ into m intervals $[0, d], [d, 2d], \dots, [(m-1) \cdot d, D]$. For each interval, $\mathcal{S}_u(i)$ and $\mathcal{P}_u(i)$ represent the clusters of SINR values that fall into interval $[(i-1) \cdot d, i \cdot d]$ and the corresponding PRR values. We use the average PRR in $\mathcal{P}_u(i)$ to approximate the PRR values, i.e.,

$$\overline{PRR}_u(i) = \frac{\sum_{SINR_u(j) \in \mathcal{S}_u(i)} PRR_u(j)}{|\mathcal{P}_u(j)|} \quad (2)$$

Under the above model, the relationship between PRR and SINR can be represented by a set of SINR-PRR points: $\{(i \cdot d, \overline{PRR}_u(i)) \mid 0 \leq i \leq m\}$. Figure 5(b) illustrates the clustered PRR-SINR models under different numbers of jammers. To compensate for system errors in the measurements, 20% outliers are removed from the results. We can see that the relationship between PRR and SINR yields a high similarity under the clustered model when the number of jammers varies.

D. Online model estimation

We now discuss how to dynamically estimate the power control and interference models. Each node periodically broadcasts N beacon messages at K power levels in turn. Each node estimates neighbors' RSS models and its own interference model. Nodes then exchange their model parameters with neighbors. Suppose node u receives J messages from neighbor v . The parameters of the RSS model of link from v to u , $A_{v,u}$ and $B_{v,u}$ as defined in (1), can be estimated by linear interpolation of the J measurements.

Accurate estimation of the PRR-SINR model incurs high overhead because the transmissions of sender and jammers must be precisely synchronized. As shown in Figure 5, the PRR-SINR model is a good approximation to the PRR-SINR model. Moreover, the PRR-SINR model can be measured without any jammers, which significantly reduces the overhead. Suppose node v receives N' out of N beacons that are sent by u with transmit power level P_t . The average noise energy is N dBm.

Then a pair of PRR-SINR values can be calculated as:

$$\begin{aligned} SINR &= RSS(v, u, P_t) - N_{dBm} \\ &= A_{u,v} \times P_t + B_{u,v} - N_{dBm} \end{aligned} \quad (3)$$

$$PRR = \frac{N'}{N} \quad (4)$$

To estimate the clustered PRR-SINR model, a node stores the average PRR for each SINR interval $[(i-1) \cdot d, i \cdot d]$. After a pair of PRR-SINR values are calculated, it is used to update the average PRR in the corresponding SINR interval.

V. DESIGN AND IMPLEMENTATION OF C-MAC

This section presents the design and implementation of C-MAC. We first provide an overview of C-MAC in Section V-A. The design of each component of C-MAC is discussed in detail from Section V-B to V-E.

A. Overview

The primary design goal of C-MAC is high system throughput, which is achieved by allowing multiple links within the interference range of each other to transmit concurrently. To mitigate the negative impact of increased interference, C-MAC carefully chooses transmit power of senders to maximize the total throughput of active links. The power adjustment is conducted based on the power control and interference models that are estimated by each node in an online fashion.

C-MAC is composed of the following components: 1) *online model estimation* that periodically estimates power control and interference models as discussed in Section IV-D; 2) *traffic snooping* that identifies transmitting links by snooping the channel; 3) *concurrency check* that examines if the pending data can be transmitted concurrently with the ongoing traffic based on the interference model; 4) *interference assessment* that obtains the interference level at the intended receiver; 5) *throughput prediction* that estimates the throughput of concurrently transmitting links and chooses the transmit power that maximizes the expected total throughput; and 6) *concurrent transmission engine* that is the core of C-MAC and coordinates the operation of other components.

Data packets in C-MAC are transmitted in *blocks*. A block is composed of multiple packets. Figure 6 shows the procedure

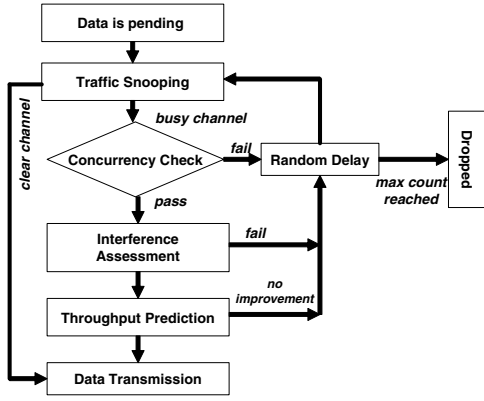


Fig. 6. The procedure of transmitting a data block in the concurrent transmission engine.

that is used by the concurrent transmission engine to transmit a block. When a node has a block pending for transmission, it first snoops the channel and identifies the current receivers within its interference region. A concurrency check is then performed based on the interference model to examine if the pending data block would significantly interfere the current receivers. In particular, the data delivery at the intended receiver should have a high probability while the ongoing transmissions in the vicinity are not significantly affected by the increased interference. If the check is passed, the node obtains the level of interference at the intended receiver through an RTS/CTS exchange. Finally, the node computes the transmit power that maximizes the total throughput of the pending and existing transmissions. If the concurrency check or RTS/CTS exchange fails, or transmitting the pending data block results in no throughput improvement, the node will attempt the transmission after a random delay. The data block will be dropped after the maximum count of attempts is reached.

The block based transmission mode used by C-MAC has two key advantages. First, it amortizes the overhead of traffic snooping and RTS/CTS exchange. Second, it reduces the complexity of several designs of C-MAC such as identifying interfering links and estimating the total throughput under interference. As a result, the probability that multiple links (within the interference range of each other) can transmit concurrently.

B. Traffic snooping

When a node tries to send a block, it first assesses the condition of channel by snooping the ongoing traffic. Traffic snooping is implemented based on two mechanisms. First, an energy-based method is used to sense the channel. If the channel is clear, the pending block is transmitted. Otherwise, C-MAC identifies the active links that are concurrently transmitting. Specifically, the node listens to the channel for T_a ms and stores the received packets in a buffer. During the T_a ms, the node periodically samples the Clear Channel Assessment (CCA) register for m times. If the average of sampled signal energies is significantly below the noise floor, the channel is clear. Otherwise, C-MAC declares the channel is busy.

If no packets are received during the T_a ms and the channel is busy, the node backs off and retries after a random delay.

In such a case, the node lies inside the interference range but outside the communication range of other sending nodes. As no information of the ongoing transmissions can be obtained, the sending node has to retry the channel access later. If at least one data packet is received, the traffic snooping completes and the *concurrency check* component will be invoked.

C. Concurrency check

The purpose of concurrency check is to estimate if the pending data block can be transmitted concurrently with ongoing transmissions. Suppose node s_0 attempts to transmit a data block to node r_0 . s_0 first examines the data packets overheard in the traffic snooping phase and identifies the active links. Suppose there exist total k active links denoted by set $K = \{(s_i, P_{s_i}, r_i) \mid 0 \leq i \leq k\}$ where s_i , P_{s_i} , r_i represent the sender, transmit power, and receiver of an active link. We note that, due to the hidden terminal problem, K does not include all the links whose transmissions collide with the transmissions from s_0 to r_0 . For each receiver r_i in set K , the sending node estimates the new PRR of r_i if it transmits at the minimum power P_0 . It first computes the new SNR at node r_i by:

$$SNR(r_i)_{dB} = RSS(r_i, s_i, P_{s_i})_{dBm} - 10 \log_{10} \left(10^{\frac{RSS(r_i, s_0, P_0)}{10}} + 10^{\frac{N_{r_i} + I_{r_i}}{10}} \right) \quad (5)$$

$$PRR(s_i, r_i) = PRR_{r_i}(SNR(r_i)) \quad (6)$$

where $RSS(r_i, s_i, P_{s_i})$ and $RSS(r_i, s_0, P_0)$ are the signal strength of the packets sent by s_i (at transmit power P_{s_i}) and s_0 (at transmit power P_0), respectively. $RSS(r_i, s_0, P_0)$ can be computed from the RSS model of the link from s_0 to r_i as $RSS(r_i, s_0, P_0) = A_{s_0, r_i} \times P_0 + B_{s_0, r_i}$, which is discussed in Section IV-B. In addition, $RSS(r_i, s_i, P_{s_i})$ and $N_{r_i} + I_{r_i}$ are carried by the data packets. After $SNR(r_i)$ is computed, the packet reception ratio of the link from s_i to r_i , $PRR(s_i, r_i)$, can then be looked up from r_i 's PRR-SNR table stored by node s_0 . Note that the estimation of $PRR(s_i, r_i)$ does not require any message exchange. If $PRR(s_i, r_i)$ is smaller than a threshold α , the concurrency check fails. That is, node s_0 cannot transmit concurrently with s_i because the PRR of the link from s_i to r_i would drop below α . If the PRRs of all links in set K are above α , the concurrency check passes and the RTS/CTS exchange is started.

D. Interference assessment

When the sender passes the concurrency check, it exchanges RTS/CTS packets with the receiver. The purpose of RTS/CTS exchange is two-fold. First, similar to the RTS/CTS exchange of traditional CSMA/CA MACs, it avoids the primary interference caused by two nodes sending to the same receiver. In addition, the sender obtains the information about the interference condition at the receiver from the exchange, which enables it to estimate the quality of the link.

Specifically, after passing the concurrency check, the sender transmits a short RTS packet that contains the ID of receiver. The receiver then responds with a short CTS packet that includes the sum of current interference and noise energy, $(N_r + I_r)$ dBm. Other nodes that attempt to transmit to the receiver will back off after hearing the RTS or CTS. Both RTS

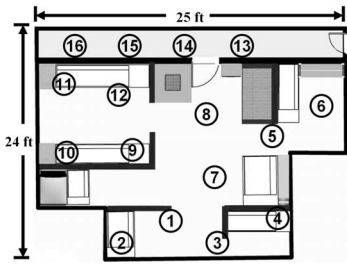


Fig. 7. A test-bed deployed in an office and a corridor.

and CTS packets are transmitted at the maximum power. If the receiver hears an RTS in the middle of receiving a data block from another node, it does not respond with the CTS packet, which avoids the primary interference.

E. Throughput prediction

After the RTS/CTS exchange, the sender estimates if its transmission will lead to the improvement of the total throughput of all active links within its interference region. Suppose node s_0 attempts to transmit a data block to node r_0 . Specifically, s_0 finds the transmit power that maximizes the improvement of throughput as follows.

$$\Delta = \max_{P_s} \sum_{i \in [0, |K|]} PRR(s_i, r_i) - |K| \quad (7)$$

where $\sum_{i \in [0, |K|]} PRR(s_i, r_i)$ is equal to the sum of PRRs of all active links (including the link from s_0 to r_0). Node s_0 assumes that all the active links in K (overheard during the traffic snooping phase) have a PRR of 100% as accurately predicting the PRR of an active link is difficult. Eqn. (7) thus represents a conservative estimation of the maximum improvement of total throughput. If Δ computed by (7) is smaller than a threshold β , s_0 will transmit a block of data with the transmit power found in (7). Otherwise, the current attempt fails. We now discuss how (7) is computed. $PRR(s_0, r_0)$ is obtained by looking up r_0 's PRR-SNR model (stored by node s_0) by using $SNR(r_0)$ that is computed as follows:

$$\begin{aligned} SNR(r_0)_{dB} &= RSS(r_0, s_0, P_s)_{dBm} - (N_{r_0} + I_{r_0})_{dBm} \\ &= A_{s_0, r_0} \times P_s + B_{s_0, r_0} - (N_{r_0} + I_{r_0})_{dBm} \quad (8) \end{aligned}$$

where $N_{r_0} + I_{r_0}$ is contained in the CTS packet from r_0 . A_{s_0, r_0} and B_{s_0, r_0} are parameters of the power control model of link from s_0 to r_0 . For the PRR of link from s_i to r_i ($i \neq 0$), $PRR(s_i, r_i)$ is computed according to (5) and (6) (where P_0 is replaced with P_s).

VI. EXPERIMENTS

A. Experimental methodology and settings

We implemented C-MAC in TinyOS-1.x and evaluated its performance on a test-bed composed of 16 Tmote Sky nodes. The test-bed is deployed in an indoor office environment shown in Figure 7. The main purpose of our performance evaluation is to demonstrate the advantage of channel concurrency at the MAC layer. To this end, we compare C-MAC with B-MAC [12] that is the default MAC protocol released in TinyOS-1.x.

Several recent MAC protocols (e.g., Funneling-MAC [1], Z-MAC [15] and X-MAC [3]) are shown to be superior to B-MAC. Despite the performance improvement, these protocols are designed based on the same channel access strategy as B-MAC, which prevents interfering nodes from accessing channel simultaneously. In contrast, the major advantage of C-MAC is to improve system throughput by concurrent transmissions. Therefore, the approaches adopted by recent MACs (e.g., shorter preambles [3], combination with TDMA [1], and opportunistic usage of idle nodes' slots [15]) are complementary to the design of C-MAC. Therefore, we only conduct performance comparison between C-MAC and B-MAC.

B-MAC supports several asynchronous sleep modes with different periods. In each sleep mode, B-MAC sets a different length of packet preamble to synchronize the sender and receiver. As C-MAC is designed to achieve high throughput when nodes are actively communicating, we disable the sleep mode of B-MAC for fair comparison. The preamble of B-MAC is set to be 4 bytes. During initialization, every node broadcasts 5 beacons at 6 different power levels (from level 5 to 30 at an increment of 5). The RSS and PRR-SNR models are updated in the end of initialization. The model estimation is continuously conducted by each node at a period of two minutes³. The traffic snooping interval is 80 ms. The PRR thresholds of concurrency check and throughput prediction are set to be $\alpha = 50\%$ and $\beta = 20\%$ (see Section V), respectively.

B. Performance with fixed block size

In this set of experiments, we compare C-MAC with B-MAC in terms of throughput, delay and energy efficiency. The following traffic pattern is used for the 16 Tmote nodes in the test-bed. Node i transmits to node $i + 1$ at the maximum rate, where $i = 1, 3, 5 \dots, 15$. In the following discussion, *Link k* refers to the link from node $2k - 1$ to node $2k$ in Figure 7. The block size is fixed to be 100 unless otherwise stated. We evaluate the performance of C-MAC and B-MAC with different block sizes in Section VI-C.

We evaluate system throughput in the first set of experiments. The throughput is calculated as the total data delivery rates of all links. As the transmit power is critical to the performance of carrier sensing, B-MAC is evaluated under four different transmit power settings. Under each setting, all the senders use the same transmit power. To examine how the system throughput evolves with the traffic load, a new link (*Link i* from node $2i - 1$ to node $2i$) starts to transmit in each run.

Figure 8(a) shows the system throughput of B-MAC and C-MAC. The default block size of B-MAC is one, i.e., the carrier sensing is conducted for each packet transmission. We observed that the block size of 100 only slightly increases the throughput of B-MAC. Thus we used the block size of 100 for only one setting (where the transmit power is -25 dBm) and the block size of one for other settings. Figure 8(a) shows several interesting observations. (1) The throughput of B-MAC remains

³In practice, the period of model estimation is determined by traffic load and the level of environmental dynamics.

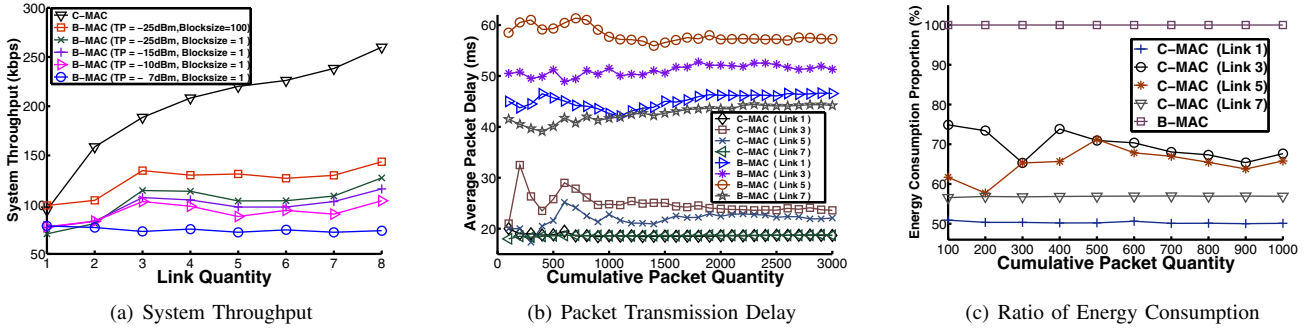


Fig. 8. Performance Evaluation when Block Size is 100.

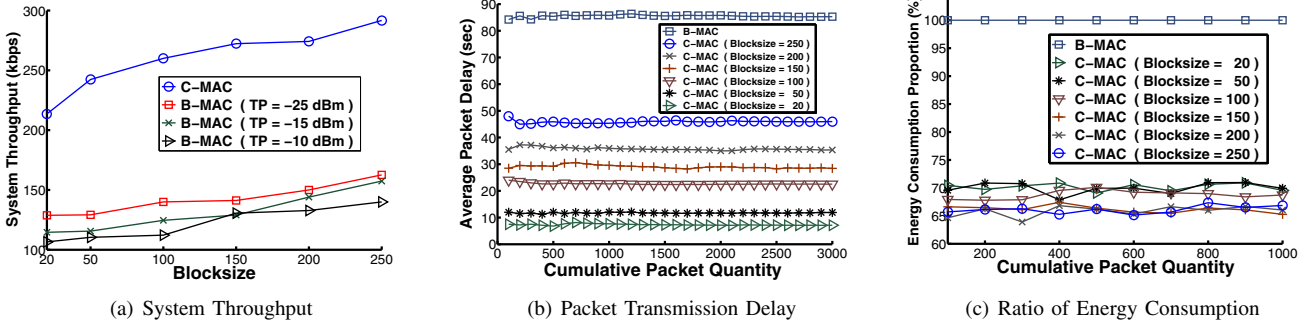


Fig. 9. Performance Evaluation when Different Block Sizes are Used.

roughly 75 kbps when a high transmit power (-7 dBm) is used. This is because all senders are within the interference range of each other and hence only one of them can access the channel at any time. As a result, the system throughput is roughly equal to the throughput of a single link. (2) When a lower transmit power is used, the system throughput of B-MAC increases to about 100 kbps when total three links are present, due to the reduced interference range. However, the system throughput starts to drop when more links become active. This is because the new links are within the interference range of existing ones, which results in a higher level of contention. When *Link 7* and *Link 8* start to transmit, the system throughput increases again as they are in the corridor (shown in Figure 7) and do not significantly interfere with other links.

Figure 8(a) shows that C-MAC achieves a system throughput of 90 ~ 260 kbps, which corresponds to a 1.2-2.6X performance gain over B-MAC. C-MAC outperforms B-MAC even when there is only one link. C-MAC performs one traffic snooping and RTS/CTS exchange for a block of packets while a CCA is needed for each packet under B-MAC. When more links are present, the performance gain of C-MAC is even greater because of the higher degree of concurrent transmissions. We note that the system throughput under C-MAC stops growing if more than 6 links were added within the room (shown in Figure 7). Similar to the case of B-MAC, *Link 7* and *Link 8* further improve the system throughput as they are in the corridor and do not significantly interfere with other links.

Figure 8(b) plots the average packet transmission delay, which is defined as the interval between the time instance

when the first packet in the block becomes the head of data buffer to the time instance when the packet is transmitted on the channel. We randomly choose four links, *Link 1*, *Link 3*, *Link 5* and *Link 7* for evaluation. We can see that the delay of B-MAC is significantly larger than that of C-MAC. For example, the delay of *Link 5* reduces from 59 ms to 21 ms, i.e., a 64% reduction, when B-MAC is replaced with C-MAC. Similar results are also observed for other links (1, 3 and 7), as shown in Figure 8(b).

Figure 8(c) shows the ratio of the network energy consumption under B-MAC and C-MAC. The energy consumption of each radio is measured as the sum of the energy consumed in each of three different radio states: idle, receiving and transmitting. We first measure the total time that the radio spends in each state by instrumenting the Tmote CC2420 radio stack. We then calculate the energy consumed in each state by multiplying the total time the radio spends in that state by the power consumed in that state. The power consumption values are all taken directly from the CC2420 data sheet. Four links (1,3,5,7) are chosen for evaluation. We denote the lowest energy consumption of all links under B-MAC as 100%. We can see that C-MAC can reduce the energy consumption of *Link 1* to 51%, *Link 3* to 70%, *Link 5* to 65%, and *Link 7* to 58%, respectively. This result shows that C-MAC can effectively save power consumption to extend the system life time.

C. Performance with different block sizes

In this set of experiments, we study the impact of block size on C-MAC performance. The block size is varied between 20 and 250. The system throughput is plotted in Figure 9 (a). We can see that C-MAC always outperforms B-MAC.

Moreover, the throughput of C-MAC increases more quickly than that of B-MAC. This is because C-MAC allows concurrent transmissions and hence the increased block size leads to the higher throughput of multiple links. On the other hand, only one link can transmit under B-MAC and hence the throughput gain due to a larger block size is limited.

Figure 9 (b) plots the average packet transmission delay of all links. We can see that the delay of C-MAC increases with block size. This is because a new block must wait the current block to be transmitted before gaining the access to the channel. We set the block size to be one for B-MAC as it leads to the lowest transmission delay. Nevertheless, the average delay of all links under B-MAC is significantly longer than that of C-MAC as B-MAC only allows one link to transmit at any time. When block size decreases from 250 to 20, the transmission delay reduction compared with B-MAC increases from 42% to 89%. Figure 9 (a) and (b) show that, although a larger block size leads to a higher system throughput, it also increases the packet transmission delay. However, C-MAC outperforms B-MAC on both throughput and delay in all block size settings.

We now evaluate the energy consumption of all nodes under C-MAC and B-MAC. B-MAC consumes the least energy when the block size is 250. We compare the energy consumption of C-MAC with different block sizes and B-MAC with block size of 250 and the ratios are plotted in Figure 9 (c). For a wide range of block sizes, C-MAC only consumes 64%~72% energy that B-MAC consumes. We can also see, although a larger block size significantly increases system throughput of C-MAC, it does not considerably impact the total energy consumption. This is because the transmission energy dominates the total energy consumption of the network and hence transmitting the same number of packets always leads to similar energy consumption despite the difference of throughput.

VII. CONCLUSION

This paper presents a new MAC protocol called C-MAC designed to achieve high-throughput bulk communication for data-intensive sensing applications. We first establish an empirical pair-wise power control model and a physical interference model that characterize the transitional region of packet reception. Nodes running C-MAC estimate the level of interference on the channel and adjust the transmission power accordingly. C-MAC employs a block-based communication mode that not only amortizes the overhead of channel concurrency assessment, but also improves the probability that multiple nodes within the interference range of each other can transmit concurrently. Our experiments based on a 16-node test-bed show that C-MAC significantly outperforms the state-of-art CSMA protocol in TinyOS on system throughput, delay, and energy consumption.

VIII. ACKNOWLEDGEMENT

The work described in this paper was partially supported by a grant from the Research Grants Council of Hong Kong Special Administrative Region, China [Project No. RGC 9041266].

REFERENCES

- [1] G.-S. Ahn, S. G. Hong, E. Miluzzo, A. T. Campbell, and F. Cuomo. Funneling-mac: a localized, sink-oriented mac for boosting fidelity in sensor networks. In *SenSys*, 2006.
- [2] M. Alicherry, R. Bhatia, and L. Li. Joint channel assignment and routing for throughput optimization in multi-radio wireless mesh networks. In *MobiCom*, 2005.
- [3] M. Buettner, G. V. Yee, E. Anderson, and R. Han. X-mac: a short preamble mac protocol for duty-cycled wireless sensor networks. In *SenSys*, 2006.
- [4] O. Chipara, C. Lu, and J. Stankovic. Dynamic conflict-free query scheduling for wireless sensor networks. In *ICNP*, 2006.
- [5] A. El-Hoiydi and J.-D. Decotignie. Wisemac: An ultra low power mac protocol for the downlink of infrastructure wireless sensor networks. In *ISCC*, 2004.
- [6] O. Goussevskaia, Y. A. Oswald, and R. Wattenhofer. Complexity in geometric sinr. In *MobiHoc*, 2007.
- [7] E.-S. Jung and N. H. Vaidya. A power control mac protocol for ad hoc networks. In *MobiCom*, 2002.
- [8] A. Kashyap, S. Ganguly, and S. R. Das. A measurement-based approach to modeling link capacity in 802.11-based wireless networks. In *MobiCom*, 2007.
- [9] A. Kashyap, S. Sengupta, R. Bhatia, and M. Kodialam. Two-phase routing, scheduling and power control for wireless mesh networks with variable traffic. In *SIGMETRICS*, 2007.
- [10] S. Lin, J. Zhang, G. Zhou, L. Gu, T. He, and J. A. Stankovic. ATPC: Adaptive Transmission Power Control for Wireless Sensor Networks. In *ACM SenSys*, 2006.
- [11] A. Muqattash and M. Krunz. Powmac: A single-channel power-control protocol for throughput enhancement in wireless ad hoc networks. *IEEE JSAC, VOL. 23, NO. 5*, 23, May 2005.
- [12] J. Polastre, J. Hill, and D. Culler. Versatile low power media access for wireless sensor networks. In *SenSys*, 2004.
- [13] V. Rajendran, K. Obraczka, and J. Garcia-Luna-Aceves. Energy-efficient, collision-free medium access control for wireless sensor networks. In *SenSys*, Los Angeles, California, USA, 2003.
- [14] C. Reis, R. Mahajan, M. Rodrig, D. Wetherall, and J. Zahorjan. Measurement-based models of delivery and interference in static wireless networks. In *SIGCOMM*, 2006.
- [15] I. Rhee, A. Warrier, M. Aia, and J. Min. Z-mac: a hybrid mac for wireless sensor networks. In *SenSys*, San Diego, California, USA, 2005.
- [16] I. Rhee, A. Warrier, J. Min, and L. Xu. Drand:: distributed randomized tdma scheduling for wireless ad-hoc networks. In *MobiHoc*, 2006.
- [17] M. Sha, G. Xing, G. Zhou, and S. Liu. C-mac: Model-driven concurrent medium access control for wireless sensor networks. Technical report, Michigan State University, 2008.
- [18] D. Son, J. Heidemann, and B. Krishnamachari. Towards concurrent communication in wireless networks. Technical Report ISI-TR-646, Information Sciences Institute, USC, 2007.
- [19] D. Son, B. Krishnamachari, and J. Heidemann. Experimental study of concurrent transmission in wireless sensor networks. In *SenSys*, 2006.
- [20] R. Szewczyk, A. Mainwaring, J. Polastre, J. Anderson, and D. Culler. An analysis of a large scale habitat monitoring application. In *SenSys*, 2004.
- [21] T. van Dam and K. Langendoen. An adaptive energy-efficient mac protocol for wireless sensor networks. In *SenSys*, 2003.
- [22] M. Vutukuru, K. Jamieson, and H. Balakrishnan. Harnessing exposed terminals in wireless networks. In *USENIX NSDI*, 2008.
- [23] N. Xu, S. Rangwala, K. K. Chintalapudi, D. Ganesan, A. Broad, R. Govindan, and D. Estrin. A wireless sensor network for structural monitoring. In *SenSys*, 2004.
- [24] W. Ye, J. Heidemann, and D. Estrin. Medium access control with coordinated, adaptive sleeping for wireless sensor networks. *IEEE/ACM Transactions on Networking*, June 2004.
- [25] W. Ye, F. Silva, and J. Heidemann. Ultra-low duty cycle mac with scheduled channel polling. In *SenSys*, 2006.
- [26] J. Zhao and R. Govindan. Understanding packet delivery performance in dense wireless sensor networks. In *SenSys*, 2003.